Multipolar Interband Absorption in a Semiconductor Quantum Dot: Electric Quadrupole Enhancement

Introduction

A quantum dot is an artificially created semiconductor structure in the size range of 5 to 100 nm. As a whole, it behaves like an atom since the quantum effects of the confined electrons are enlarged with respect to the interactions of the electrons inside each atom. Since the conception of quantum dots in the early 1980s, the study of their physical properties continues to be a very active field of research. Quantum dots can now be synthesized by various methods and have a multitude of potential technological applications, which include lasers with high optical gain and narrow bandwidth, and wavelength tunability.[1] Also, dipole–dipole interaction between neighboring quantum dots is being explored for applications in quantum computing.[2] Furthermore, quantum dots are potential single-photon sources, which may be used to create nonclassical electromagnetic states.[3]

Near-field optical techniques have extended the range of optical measurements beyond the diffraction limit and stimulated interests in many disciplines, especially material sciences and biological sciences.[4,5] Spatial resolution is increased by accessing evanescent modes in the electromagnetic field. These modes are characterized by high spatial frequencies and therefore enable the probing of subwavelength structures. Near-field optical techniques have also been employed to study the optical properties and dynamics of charge carriers in artificial nanostructures such as quantum wells, quantum wires, and quantum dots (see, for example, Refs. 6–8).

Nanostructures interacting with optical near fields do not necessarily behave in the same way as nanostructures interacting with far-field radiation. In Ref. 9, for example, the response of a quantum well when excited by the diffracted field of an aperture enhances quadrupole transitions, giving rise to a modified absorption spectrum of the quantum well. Furthermore, absorption properties may also be modified due to nonlocal spatial dispersion as described in Ref. 10. Recently, Knorr *et al*. formulated a general theoretical, self-consistent multipolar formalism for solids. This formalism can even be extended to account for delocalized charges.[11] The spectral response originating from the interaction between semiconductor quantum dots and the optical field generated by a small aperture has been discussed in Refs. 12–14. References 13 and 14 account for the highly inhomogeneous excitation field produced by the subwavelength aperture.

This article focuses on the interaction of a spherical semiconductor quantum dot with a highly confined optical near field. It has been shown that such fields can be generated near laser-illuminated, sharp-pointed tips.[15–17] Here, we adopt this geometry and approximate the fields near the tip by an oscillating electric dipole oriented along the tip axis. In Ref. 18, it has been demonstrated that this is a reasonable approximation and that the dipole moment can be related to the computationally determined field-enhancement factor. Furthermore, our analysis relies only on the field distribution and not on the actual enhancement factor. We will consider a spherical quantum dot in the strong-confinement limit.

The interaction between a quantum dot and the optical near field is described semiclassically using the multipolar expansion. For far-field excitation, the first term in this expansion, the electric dipole term, gives rise to a response that is considerably stronger than the response produced by subsequent terms. This is due to the fact that the physical dimension of the quantum dot is much smaller than the wavelength of optical radiation and also due to the weak spatial variation of the exciting far field. The spatial variations of optical near fields, however, are much stronger, and, as a consequence, it is expected that the contribution of higher terms in the multipolar expansion cannot *a priori* be neglected. In this article, the strength of electric quadrupole absorption compared with the strength of the electric dipole absorption will be analyzed. This study is motivated by two basic questions: (1) To what extent are standard selection rules modified by higher-order multipolar transitions in confined optical fields? and (2) Can optical resolution be improved by selectively exciting higher-order multipole transitions? To keep the analysis as simple as possible, we will neglect the Coulomb interaction between hole and electron as well as the spin of these particles.

The article is organized as follows: In the next section, the semiclassical multipolar Hamiltonian formalism is presented. In the same section, the wave functions for the hole and the electron in an ideal spherical quantum dot are reviewed, and the field operator representation is outlined. In subsequent sections, the absorption rate in the electric dipole approximation is discussed, and the absorption rate arising from the electric quadrupole term in the multipolar expansion is derived. The theory is applied to a quantum dot near a laser-illuminated metal tip. Approximated parameters for GaAs are used to estimate the absorption rate for electric dipole transitions and electric quadrupole transitions. In the last section, results are discussed and conclusions and future work are presented.

Preliminary Concepts

1. The Multipolar Hamiltonian

A semiclassical approach is used to describe the interaction of a quantum dot with the electromagnetic field. In this approach, the electromagnetic field obeys the Maxwell equations, and the Hamiltonian of the system $(\hat{H})$ can be separated into two contributions as

$$\hat{H} = \hat{H}_0 + \hat{H}_I, \qquad (1)$$

where $\hat{H}_0$ and $\hat{H}_I$ are the unperturbed Hamiltonian (absence of fields) and the interaction Hamiltonian, respectively. In the Coulomb gauge, they are defined as

$$\hat{H}_0 = \frac{1}{2m}\hat{\mathbf{p}}^2 + V(\mathbf{r}), \qquad (2)$$

$$\hat{H}_I = -\frac{e}{m}\hat{\mathbf{p}}\cdot\mathbf{A}(\mathbf{r},t) + \frac{e^2}{2m}\mathbf{A}^2(\mathbf{r},t) + e\phi(\mathbf{r},t), \qquad (3)$$

where $V(\mathbf{r})$ is the potential energy, $\hat{\mathbf{p}}$ is the canonical momentum, $\mathbf{A}(\mathbf{r},t)$ is the vector potential, and $\phi(\mathbf{r},t)$ is the scalar potential. The multipolar Hamiltonian is obtained by using the canonical transformation $\hat{U} = \exp(iz/\hbar)$ in which z is given by[19,20]

$$z = \int \tilde{\mathbf{P}}(\mathbf{r})\cdot\mathbf{A}(\mathbf{r},t)d^3r \equiv 0, \qquad (4)$$

where $\tilde{\mathbf{P}}(\mathbf{r})$ is the polarization. If the vector potential $\mathbf{A}(\mathbf{r},t)$ and the scalar potential $\phi(\mathbf{r},t)$ are expanded in a Taylor series

with respect to a reference charge distribution at $\mathbf{R}$ as follows:

$$\mathbf{A}(\mathbf{r},t) = \sum_{n=0}^{\infty} \frac{1}{(n+2)n!}\left[(\mathbf{r}-\mathbf{R})\cdot\nabla\right]^n \mathbf{B}(\mathbf{R},t)\cdot(\mathbf{r}-\mathbf{R}), \quad (5)$$

$$\phi(\mathbf{r},t) = \sum_{n=0}^{\infty} \frac{-1}{(n+1)!}(\mathbf{r}-\mathbf{R})\left[(\mathbf{r}-\mathbf{R})\cdot\nabla\right]^n \cdot\mathbf{E}(\mathbf{R},t), \quad (6)$$

then this choice of $\mathbf{A}(\mathbf{r},t)$ and $\phi(\mathbf{r},t)$ satisfies condition (4). By substituting Eqs. (5) and (6) into Eq. (3), we obtain

$$\hat{H}_I = \hat{H}^E + \hat{H}^M + \hat{H}^Q + \dots. \qquad (7)$$

Here $\hat{H}^E$, $\hat{H}^M$, and $\hat{H}^Q$ are the first three terms of the multipolar expansion, namely, the electric dipole, the magnetic dipole, and the electric quadrupole, respectively, which are defined as

$$\hat{H}^E = -\mathbf{d}\cdot\mathbf{E}(\mathbf{r},t)\big|_{\mathbf{r}=\mathbf{R}}, \qquad (8a)$$

$$\hat{H}^M = -\mathbf{m}\cdot\mathbf{B}(\mathbf{r},t)\big|_{\mathbf{r}=\mathbf{R}}, \qquad (8b)$$

$$\hat{H}^Q = -\nabla_1\cdot\overleftrightarrow{\mathbf{Q}}\mathbf{E}(\mathbf{r}_1,t)\big|_{\mathbf{r}_1=\mathbf{R}}, \qquad (8c)$$

where $\mathbf{d}$, $\mathbf{m}$, and $\overleftrightarrow{\mathbf{Q}}$ are the electric dipole moment, the magnetic dipole moment, and the electric quadrupole moment, respectively, with respect to a reference charge distribution at $\mathbf{R}$. The nabla operator ∇_1 acts only on the spatial coordinates $\mathbf{r}_1$ of the electric field. It is important to mention that $\mathbf{m}$ depends on the canonical momentum. For weak fields, however, the canonical momentum can be approximated as the mechanical momentum.

2. The Quantum Dot Wave Functions (Strong Confinement)

We assume that a spherical quantum dot is made of a direct band-gap semiconductor for which the bulk electric dipole transitions are allowed between the valence band and the conduction band. In a generic manner, we assume that the valence band has p-like character and the conduction band has s-like character. The latter assumption is commonly encountered for several semiconductors such as the GaAs. We consider that an electron and a hole are completely confined in a sphere with radius a by the potential energy

$$V(r) = \begin{cases} 0 & r \le a \\ \infty & r > a \end{cases}, \qquad (9)$$

where r is the radial coordinate. Also, we assume that the electron (hole) has the same effective mass m_e (m_h) as in the bulk material. This consideration is valid if the volume of the sphere is much larger than the volume of a primitive cell in the crystal. Strong confinement is achieved if the Bohr radii of electron (b_e) and hole (b_h) are much larger than the radius of the quantum dot a. By assuming the aforementioned conditions, the wave function of the electron in the conduction band can be expressed as

$$\Psi^e(\mathbf{r}) = \frac{1}{\sqrt{V_0}} u_{c,0}(\mathbf{r}) \zeta^e(\mathbf{r}). \qquad (10)$$

Here $u_{c,0}(\mathbf{r})$ is the conduction-band Bloch function (with lattice periodicity) having the corresponding eigenvalue $k = 0$, and V_0 is the volume of the *unit cell*. Similarly, the corresponding wave function for the hole in the valence band is

$$\Psi^h(\mathbf{r}) = \frac{1}{\sqrt{V_0}} u_{v,0}(\mathbf{r}) \zeta^h(\mathbf{r}), \qquad (11)$$

with $u_{v,0}(\mathbf{r})$ being the valence-band Bloch function with eigenvalue $k = 0$. $\zeta^e(\mathbf{r})$ and $\zeta^h(\mathbf{r})$ are the envelope functions, which vary spatially much slower than $u_{v,0}(\mathbf{r})$ and $u_{c,0}(\mathbf{r})$. Roughly, the energy difference between adjacent electron {hole} energy levels is

$$\left(\hbar^2 / m_e a^2 \right) \left[\hbar^2 / \left(m_h a^2 \right) \right].$$

If this energy difference is much larger than the Coulomb interaction $e^2 / \left(4\pi \varepsilon_0 \in a^2 \right)$, the electron–hole interaction can be neglected. Under this assumption, the envelope function $\zeta^{e(h)}(\mathbf{r})$ for the electron (hole) satisfies the time-independent Schrödinger equation in which the potential energy is given by Eq. (9). The solution in spherical coordinates (r, θ, ϕ) is given by

$$\zeta_{n,l,m}^{e(h)}(r,\theta,\phi) = \Lambda_{nl}(r) Y_{l,m}(\theta,\phi). \qquad (12)$$

Here $Y_{l,m}(\theta, \phi)$ is the spherical harmonics and the radial function $\Lambda_{nl}(r)$ is

$$\Lambda_{nl}(r) = \sqrt{\frac{2}{a^3}} \frac{1}{j_{l+1}(\beta_{nl})} j_l\left(\beta_{nl} \frac{r}{a} \right). \qquad (13)$$

j_l is the lth-order spherical Bessel function, β_{nl} is the nth root of j_l, i.e., $j_l(\beta_{nl}) = 0$. The corresponding energy levels $\varepsilon^{e,h}$ are found to be

$$\varepsilon^e = \varepsilon_g + \frac{\hbar^2}{2m_e}\left(\frac{\beta_{nl}}{a} \right)^2, \qquad (14)$$

$$\varepsilon^h = \frac{\hbar^2}{2m_h}\left(\frac{\beta_{nl}}{a} \right)^2, \qquad (15)$$

where ε_g is the bulk energy band gap. Figure 91.44 shows the resulting level scheme. According to Eqs. (14) and (15), the energy is independent of the quantum number m, thus the energy level nl is ($2l+1$)-fold degenerate.
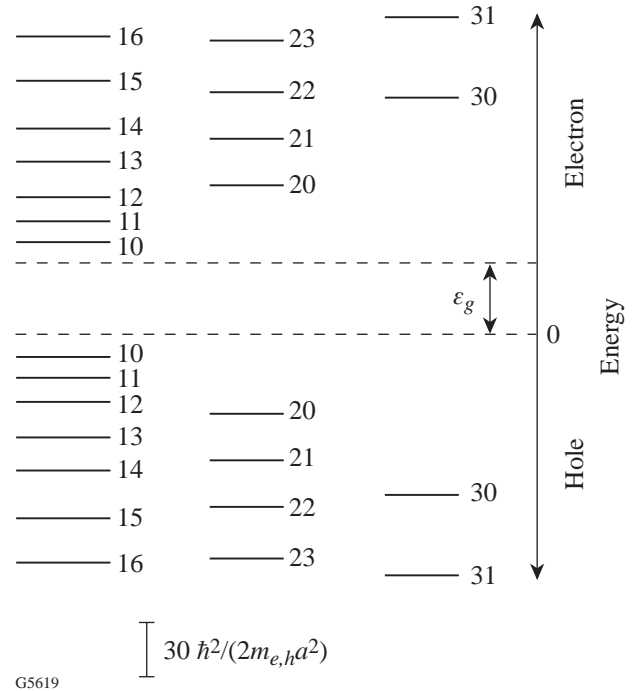

G5619

Figure 91.44
Energy level diagram of a spherical quantum dot according to Eqs. (14) and (15). Each energy level is characterized by the quantum numbers n and l, and its degeneracy corresponds to the quantum number m. Unlike the case of a hydrogen atom, the quantum number n does *not* restrict the number of suborbitals l.

3. Field Operator Representation

The annihilation carrier field operator $\hat{\Psi}$ can be expressed as a linear combination of hole creation operators in the valence band and electron annihilation operators in the conduction band, i.e.,[21,22]

$$\hat{\Psi}(\mathbf{r}) = \sum_{n,l,m}\left[\frac{1}{\sqrt{V_0}}u_{c,0}(\mathbf{r})\zeta_{nlm}^e(\mathbf{r})\hat{f}_{nlm} + \frac{1}{\sqrt{V_0}}u_{v,0}(\mathbf{r})\zeta_{nlm}^h(\mathbf{r})\hat{g}_{nlm}^\dagger\right],$$

(16)

where $\hat{f}_{nlm}$ is the annihilation operator for an electron in the conduction band with envelope function $\zeta_{nlm}^e(\mathbf{r})$. On the other hand, $\hat{g}_{nlm}^\dagger$ is the creation operator for a hole in the valence band with envelope function $\zeta_{nlm}^h(\mathbf{r})$. The creation carrier field operator $\hat{\Psi}^\dagger$ is the adjoint of Eq. (16).

Absorption in the Electric Dipole Approximation

We consider a monochromatic electric field oscillating with frequency ω as

$$\mathbf{E}(\mathbf{r},t) = \tilde{\mathbf{E}}(\mathbf{r})e^{-i\omega t} + \text{c.c.}$$

(17)

Here $\tilde{\mathbf{E}}(\mathbf{r})$ is the spatial complex amplitude and "c.c." means complex conjugate. By setting the origin O at the center of the quantum dot and using the rotating-wave approximation, the electric dipole transition rate α^E for photon absorption is[21,22]

$$\alpha^E = K_e \sum_{nml}\sum_{rst} \tilde{\delta}_{nr}\tilde{\delta}_{ls}\tilde{\delta}_{mt}\ \delta\left[\hbar\omega - \left(\varepsilon_{nl}^e + \varepsilon_{rs}^h\right)\right],$$

(18)

where $\tilde{\delta}$ is the Kronecker delta, δ is the Dirac delta function, and K_e is the absorption strength given by

$$K_e = \frac{2\pi}{\hbar}e^2\left|\tilde{\mathbf{E}}(\mathbf{0})\cdot\mathbf{P}_{cv}\right|^2,$$

(19)

and

$$\mathbf{P}_{cv} = \frac{1}{V_0}\int_{\text{UC}}u_{c,0}^*(\mathbf{r}')\mathbf{r}'u_{v,0}(\mathbf{r}')d^3r' = -\frac{\hbar}{m_0\omega}\mathbf{m}_{cv}.$$

(20)

Here $\mathbf{m}_{cv}$ is defined as

$$\mathbf{m}_{cv} \equiv \frac{1}{V_0}\int_{\text{UC}}u_{c,0}^*(\mathbf{r}')\nabla'u_{v,0}(\mathbf{r}')d^3r',$$

(21)

with UC denoting the volume of the unit cell. In Eq. (20), we have used the fact that $\hat{\mathbf{r}} \equiv -i\hat{\mathbf{p}}/m_0\omega$ (m_0 and e are the rest mass and the charge of the electron, respectively). From Eq. (18), we notice that the absorption strength (K_e) depends *only* on the bulk material properties of the quantum dot. That is, it depends on the Bloch functions u_{co} and u_{vo} and is not influenced by the envelope functions $\zeta_{nlm}^{e,h}(\mathbf{r})$. Also, Eq. (18) indicates that the allowed transitions are those for which electron and hole have the same quantum numbers, i.e.,

$$n = r \text{ and } l = s \text{ and } m = t.$$

These relationships define the selection rules for electric dipole transitions in a semiconductor quantum dot.

Absorption Arising from the Quadrupole Term

1. Electric Quadrupole Hamiltonian

The electric quadrupole interaction Hamiltonian $\hat{H}^Q$ can be represented as

$$\hat{H}^Q = \int\hat{\Psi}^\dagger(\mathbf{r})H^Q(\mathbf{r})\Psi(\mathbf{r})d^3r,$$

(22)

$$H^Q(\mathbf{r}) = -\nabla_1 \cdot \overleftrightarrow{\mathbf{Q}}(\mathbf{r})\mathbf{E}(\mathbf{r}_1,t)\big|_{\mathbf{r}_1=0},$$

(23)

where the $\overleftrightarrow{\mathbf{Q}}(\mathbf{r})$ is the quadrupole moment

$$\overleftrightarrow{\mathbf{Q}}(\mathbf{r}) = \frac{1}{2}e\mathbf{r}\mathbf{r}.$$

(24)

Here, and in the following, the subsequent listing of two vectors [as in Eq. (24)] denotes the outer product (dyadic product). The *interband* terms are found by substituting Eq. (16) and its adjoint into Eq. (22), thus

$$\hat{H}^Q = -\nabla_1 \cdot \left[\sum_{nlm} \sum_{rst} \hat{f}_{nlm}^\dagger \hat{g}_{rst}^\dagger \int u_{c,0}^*(\mathbf{r}) \right.$$

$$\times \zeta_{nlm}^{e*}(\mathbf{r}) \overleftrightarrow{\mathbf{Q}}(\mathbf{r}) u_{v,0}(\mathbf{r}) \zeta_{rst}^h(\mathbf{r}) d^3 r \Big]$$

$$\times \mathbf{E}(\mathbf{r}_1,t)\Big|_{\mathbf{r}_1=0} + \text{h.c.}, \tag{25}$$

where "h.c." denotes the Hermitian conjugate. We calculate the integral of Eq. (25) by decomposing it into a sum of integrals over the volume occupied by each of the unit cells. By applying the coordinate transformation $\mathbf{r}' = \mathbf{r}-\mathbf{R}_q$, where $\mathbf{R}_q$ is a translational lattice vector (the lattice remains unchanged when it is translated by $\mathbf{R}_q$), Eq. (25) becomes

$$\hat{H}^Q = -\nabla_1 \cdot \left[e \sum_{nlm} \sum_{rst} \sum_q \hat{f}_{nlm}^\dagger \hat{g}_{rst}^\dagger \int_{\text{UC}} u_{c,0}^*\left(\mathbf{r}'+\mathbf{R}_q\right) \right.$$

$$\times \zeta_{nlm}^{e*}\left(\mathbf{r}'+\mathbf{R}_q\right)$$

$$\times \overleftrightarrow{\mathbf{Q}}\left(\mathbf{r}'+\mathbf{R}_q\right) u_{v,0}\left(\mathbf{r}'+\mathbf{R}_q\right)$$

$$\times \zeta_{rst}^h\left(\mathbf{r}'+\mathbf{R}_q\right) d^3 r' \Big] \mathbf{E}(\mathbf{r}_1,t)\Big|_{\mathbf{r}_1=0} + \text{h.c.} \tag{26}$$

Since $u_{i,0}$ ($\mathbf{r}' + \mathbf{R}_q$) = $u_{i,0}(\mathbf{r}')$ ($i = c,v$), and the functions $\zeta_{nlm}^h\left(\mathbf{r}'+\mathbf{R}_q\right)$ and $\zeta_{nlm}^e\left(\mathbf{r}'+\mathbf{R}_q\right)$ are practically constant in each unit cell volume, Eq. (26) can be approximated as

$$\hat{H}^Q \approx -\nabla_1 \cdot \left[e \sum_{nlm} \sum_{rst} \sum_q \hat{f}_{nlm}^\dagger \hat{g}_{rst}^\dagger \zeta_{nlm}^{e*}\left(\mathbf{R}_q\right) \zeta_{rst}^h\left(\mathbf{R}_q\right) \right.$$

$$\times \left(\frac{1}{2}\mathbf{R}_q\mathbf{P}_{cv} + \frac{1}{2}\mathbf{P}_{cv}\mathbf{R}_q + \overleftrightarrow{\mathbf{Q}}_{cv} \right) \Big] \mathbf{E}(\mathbf{r}_1,t)\Big|_{\mathbf{r}_1=0} + \text{h.c.} \tag{27}$$

Here $\mathbf{P}_{cv}$ is given by Eq. (20), and $\overleftrightarrow{\mathbf{Q}}_{cv}$ is defined as

$$\overleftrightarrow{\mathbf{Q}}_{cv} = \frac{1}{2V_0} \int_{\text{UC}} u_{c,0}^*(\mathbf{r}')\mathbf{r}'\mathbf{r}' u_{v,0}(\mathbf{r}') d^3 r' . \tag{28}$$

The term containing $\mathbf{R}_q\mathbf{R}_q$ has vanished because of the orthogonality of the Bloch functions, i.e., $\langle u_{i,0}|u_{j,0}\rangle = \hat{\delta}_{ij}$; $j = c,v$. The $\overleftrightarrow{\mathbf{Q}}_{cv}$ vanishes since we are assuming that the valence band is *p*-like and the conduction band is *s*-like. Thus, using $\overleftrightarrow{\mathbf{Q}}_{cv} = 0$, and replacing $\Sigma_q \to \int dR$, Eq. (27) becomes

$$\hat{H}^Q = -\nabla_1 \cdot \left[e \sum_{nlm} \sum_{rst} \hat{f}_{nlm}^\dagger \hat{g}_{rst}^\dagger \right.$$

$$\times \left(\frac{1}{2}\mathbf{P}_{cv}\mathbf{D}_{nmlrst} + \frac{1}{2}\mathbf{D}_{nmlrst}\mathbf{P}_{cv} \right) \Big]$$

$$\times \mathbf{E}(\mathbf{r}_1,t)\Big|_{\mathbf{r}_1=0} + \text{h.c.} \tag{29}$$

Here $\mathbf{D}_{nmlrst}$ is defined as

$$\mathbf{D}_{nmlrst} \equiv \int \zeta_{nlm}^{e*}(\mathbf{R})\mathbf{R}\zeta_{rst}^h(\mathbf{R}) d^3 R, \tag{30}$$

with the integration running over the volume of the quantum dot. Equation (29) is the final expression for the electric quadrupole Hamiltonian $\hat{H}^Q$. The factor $\mathbf{D}_{nmlrst}$ depends only on the envelope functions. By using the definition of $\zeta_{nlm}^{e,h}(\mathbf{R})$ given by Eq. (12), $\mathbf{D}_{nmlrst}$ becomes

$$\mathbf{D}_{nmlrst} = A_{nlrs} B_{lm} B_{st} \left\{ \frac{C_{st}}{2(2l+1)} \left[\mathbf{n}_x \pm i\mathbf{n}_y \right] \right.$$

$$\times \left\{ \tilde{\delta}_{(m+1)t} \left[\tilde{\delta}_{l(s-1)} + \tilde{\delta}_{l(s+1)} \right] \right.$$

$$+ \tilde{\delta}_{(m-1)t} \left[(l-m+1)(l-m+2)\tilde{\delta}_{l(s-1)} \right.$$

$$\left. - (l+m)(l+m-1)\tilde{\delta}_{l(s+1)} \right] \right\}$$

$$\left. + \mathbf{n}_z C_{lm} \tilde{\delta}_{mt} \left[\frac{l+m+1}{2l+3} \tilde{\delta}_{l(s-1)} + \frac{l-m}{2l-1} \tilde{\delta}_{l(s+1)} \right] \right\}, \qquad (31)$$

where the coefficients A_{nlrs}, B_{lm}, and C_{lm} are given by

$$A_{nlrs} \equiv 2\pi \int_0^a R^3 \Lambda_{nl}(R) \Lambda_{rs}(R) dR, \qquad (32a)$$

$$B_{lm} \equiv \sqrt{\frac{(2l+1)}{4\pi} \frac{(l-m)!}{(l+m)!}}, \qquad (32b)$$

$$C_{lm} \equiv \frac{2(l+m)!}{(2l+1)(l-m)!}. \qquad (32c)$$

2. Electric Quadrupole Selection Rules and Absorption Rate

Using again the Fermi Golden Rule, the electric quadrupole transition rate (α^Q) for photon absorption reads as

$$\alpha^Q = \frac{2\pi}{\hbar} \sum_{nlm} \sum_{rst} \left| \left\langle nml; rst \left| \hat{H}^Q_{\text{int}} \right| 0 \right\rangle \right|^2 \delta \left[\hbar\omega - \left(\varepsilon^e_{nl} + \varepsilon^h_{rs} \right) \right]. \qquad (33)$$

Here $|0\rangle$ is the ground state of the quantum dot. By substituting Eq. (29) into Eq. (33), we obtain that the electric quadrupole transition rate

$$\alpha^Q = \frac{2\pi}{\hbar} e^2$$

$$\times \sum_{nlm} \sum_{rst} \left| \nabla_1 \cdot \left(\frac{1}{2} \mathbf{P}_{cv} \mathbf{D}_{nmlrst} + \frac{1}{2} \mathbf{D}_{nmlrst} \mathbf{P}_{cv} \right) \tilde{\mathbf{E}}(\mathbf{r}_1) \Big|_{\mathbf{r}_1=0} \right|^2$$

$$\times \delta \left[\hbar\omega - \left(\varepsilon^e_{nl} + \varepsilon^h_{rs} \right) \right]. \qquad (34)$$

We find that the electric quadrupole absorption rate contains the dyadic product of $\mathbf{P}_{cv}$ and $\mathbf{D}_{nmlrst}$ and vice versa. While $\mathbf{P}_{cv}$ depends on the bulk material properties, $\mathbf{D}_{nmlrst}$ depends on the quantum dot properties [see Eqs. (20) and (31)]. This term implies that the allowed electric quadrupole transitions occur when the quantum numbers l, s, m, and t fulfill

$$m - t = \pm 1 \text{ and } l - s = \pm 1$$

or

$$m - t = 0 \text{ and } l - s = \pm 1.$$

These relationships form the selection rules for the electric quadrupole transitions in a semiconductor quantum dot. Figure 91.45 illustrates the first few allowed quadrupole transi-
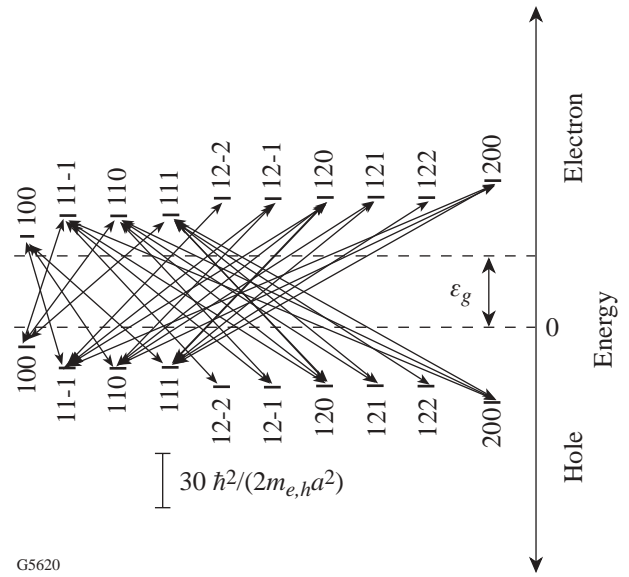
G5620

Figure 91.45

Diagram of the allowed electric quadrupole transitions in a spherical quantum dot. The energy levels are labeled by the quantum numbers *nlm* (electron) and *rst* (hole). The selection rules are $l-s = \pm 1$ and ($m-t = \pm 1$ or $m-t = 0$)]. The allowed electric quadrupole transitions exclude the allowed electric dipole transitions.

tions. We find that the quadrupole selection rules exclude any electric dipole allowed transitions. This allows the electric quadrupole transitions to be spectroscopically separated from electric dipole transitions.

Absorption Rates in Strongly Confined Optical Fields

To compare the electric dipole and electric quadrupole absorption rates in strongly confined optical fields, we consider a quantum dot in the vicinity of a laser-illuminated metal tip. This situation is encountered in so-called "apertureless" schemes of near-field optical microscopy. Strongest light confinement is achieved when the metal tip is irradiated with light polarized along the tip axis. For this situation, Fig. 91.46(a) shows the field distribution $\left(|\mathbf{E}|^2\right)$ rigorously calculated by the multiple multipole (MMP) method[23] near a gold tip with 10-nm end diameter and irradiated with $\lambda = 800$-nm light.[24] In MMP, electromagnetic fields are represented by a series expansion of known analytical solutions of Maxwell equations. To determine the unknown coefficients in the series expansion, boundary conditions are imposed at discrete points on the interfaces between adjacent homogeneous domains. The calculated field distribution, for our particular geometry, can be well approximated by the field generated by an electric dipole aligned along the tip axis z and located at the origin of tip curvature. Figure 91.46(b) demonstrates the validity of this dipole approximation: the rigorously calculated field strength

$\left(|\mathbf{E}|^2\right)$ for the metal tip is plotted along the z axis (solid line) and compared with the corresponding field generated by the dipole (dashed line).[18] The only adjustable parameter is the dipole moment $\mathbf{p}_0$, which can be related to the computationally determined field enhancement factor. Because of this very good approximation, we simply replace the laser-illuminated metal tip by a dipole.

The electric field $\mathbf{E}(\mathbf{r})$ generated by an oscillating electric dipole with moment $\mathbf{p}_0$ located at $\mathbf{r}_0$ and oscillating at the angular frequency ω can be represented as

$$\tilde{\mathbf{E}}(\mathbf{r}) = \frac{k_0^2}{\varepsilon_0} \overleftrightarrow{\mathbf{G}}(\mathbf{r},\mathbf{r}_0,\omega)\mathbf{p}_0. \tag{35}$$

Here, $k_0 = \omega/c$ (c being the vacuum speed of light), and $\overleftrightarrow{\mathbf{G}}(\mathbf{r},\mathbf{r}_0,\omega)$ is the free-space dyadic Green's function.[25] We consider the situation depicted in Fig. 91.47, where a sharp metal tip illuminated with light polarized along the tip axis (z axis) is substituted by a dipole with magnitude p_0 and oriented in the z direction. The dipole is located at $\mathbf{r}_0 = z_0\mathbf{n}_z$, and the quantum dot coordinates are $\mathbf{r} = x\mathbf{n}_x + y\mathbf{n}_y$. The quantum dot is scanned in the plane $z = 0$, while the position of the exciting dipole is kept fixed.
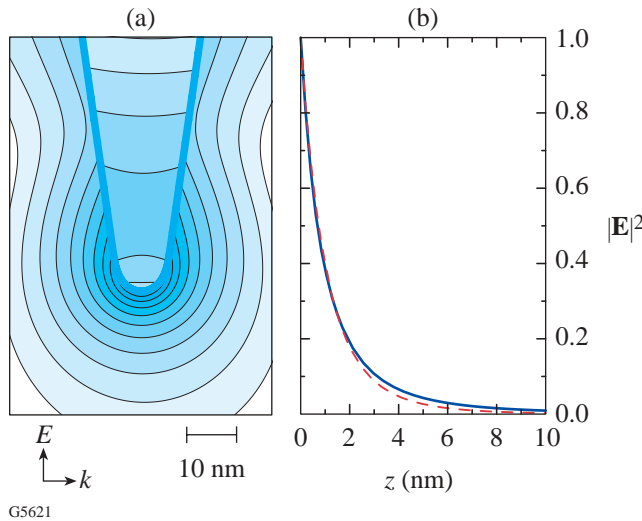

G5621

Figure 91.46
(a) Computed field distribution ($|\mathbf{E}|^2$) near a gold tip irradiated by a plane wave polarized along the tip axis. Logarithmic scaling with a factor of 2 between successive contour lines. (b) Comparison of the computed field ($|\mathbf{E}|^2$, solid curve) with the corresponding field of a dipole ($|\mathbf{E}|^2$, dashed curve) oriented along the tip axis and located inside the tip. Both fields are evaluated along the tip axis z with $z = 0$ coinciding with the tip surface.
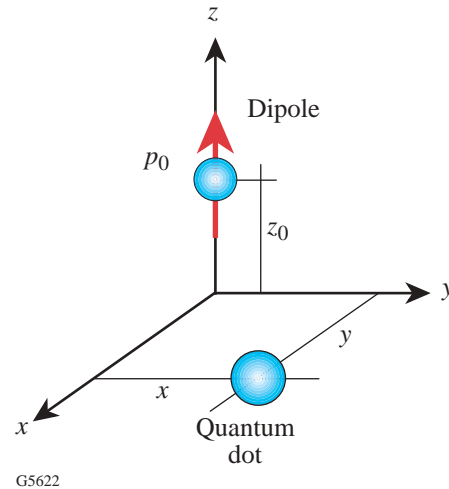

G5622

Figure 91.47
Simplified configuration of a quantum dot $\left(\mathbf{r} = x\mathbf{n}_x + y\mathbf{n}_y\right)$ interacting with a laser-illuminated metal tip. The tip is replaced by a vertical dipole $\left(\mathbf{r}_0 = z_0\mathbf{n}_z\right)$ with moment p_0 and oriented along the z axis.

To calculate the electric quadrupole absorption rate (α^Q) and the electric dipole absorption rate (α^E), we consider Bloch functions for the valence band and conduction band that are similar to those of GaAs. If we ignore spin-orbit coupling and spin degeneracy, the p-like valence band is three-fold degenerate. The Bloch functions are calculated by using the empirical pseudopotential method with parameters taken from Ref. 26. GaAs has a lattice constant of $d = 0.565$ nm, and the effective masses of electron and hole are $m_e = 0.067\,m_0$ and $m_h = 0.080\,m_0$ (light hole), respectively. Inclusion of the heavy hole will only shift the hole energy levels, as long as the heavy-hole Bohr radius is larger than the quantum dot radius.

We consider the lowest-allowed electric dipole transition, i.e., the transition with the lowest-allowed energy difference between initial and final states. During this transition, an electron with quantum numbers (100) and a hole with quantum numbers (100) are created. Since there is *no* preferential coordinate axis, we take the rotational average of Eq. (18). Also, by taking into account the degeneracy of the valence band (three-fold), the averaged electric dipole absorption rate becomes

$$\left\langle \alpha^E \right\rangle = \left\langle K_e \right\rangle \delta \left[\hbar\omega - \left(\varepsilon_{10}^e + \varepsilon_{10}^h \right) \right], \qquad (36)$$

where

$$\left\langle K_e \right\rangle = \frac{2\pi}{\hbar} e^2 \left| \tilde{\mathbf{E}}(\mathbf{0}) \right|^2 |\mathbf{P}|^2 \qquad (37)$$

and

$$|\mathbf{P}| = \left| \mathbf{P}_{cv_1} \right| = \left| \mathbf{P}_{cv_2} \right| = \left| \mathbf{P}_{cv_3} \right|. \qquad (38)$$

By computing numerically the integral of Eq. (20) over a *unit cell* of the crystal, we obtain that $|\mathbf{P}| \approx 0.75\,d$.

The lowest-energy-allowed electric quadrupole transition creates a hole with quantum numbers (110), (11-1), or (111) (three-fold degeneracy) and an electron with quantum numbers (100). Again, there is *no* preferential coordinate axis, so the rotational average of Eq. (34) has to be evaluated. Since the electric quadrupole moment is the dyadic product of two vectors with independent orientations, the rotational average of Eq. (34) is obtained in a straightforward manner. After evaluating the average and taking into account the degeneracy

of the valence band and the hole energy level, the averaged electric quadrupole absorption rate becomes

$$\left\langle \alpha^Q \right\rangle = \left\langle K^Q \right\rangle \delta \left[\hbar\omega - \left(\varepsilon_{10}^e + \varepsilon_{11}^h \right) \right]. \qquad (39)$$

Here $\left\langle K^Q \right\rangle$ corresponds to

$$\left\langle K^Q \right\rangle = \frac{2\pi}{\hbar} \frac{e^2}{2} |\mathbf{P}|^2 |\mathbf{D}|^2$$

$$\times \sum_{i,j} \left[\left| \frac{\partial}{\partial x_i} \tilde{E}_j(\mathbf{0}) \right|^2 + \frac{\partial}{\partial x_i} \tilde{E}_j(\mathbf{0}) \frac{\partial}{\partial x_j} \tilde{E}_i^*(\mathbf{0}) \right]. \qquad (40)$$

The ith Cartesian coordinate is denoted by x_i and $\tilde{E}_i(\mathbf{r})$ is ith Cartesian component of the electric field $\tilde{\mathbf{E}}_i(\mathbf{r})$. $|\mathbf{D}|$ corresponds to

$$|\mathbf{D}| = |\mathbf{D}_{10010}| = |\mathbf{D}_{100111}| = |\mathbf{D}_{10011-1}|. \qquad (41)$$

The integration of Eq. (41) over the quantum dot volume renders a value $|\mathbf{D}| \approx 0.3\,a$.

Discussion of the Near Field–Quantum Dot Interaction

We analyze absorption rates for quantum dots with the two different radii: $a = 5$ nm and $a = 10$ nm. For $a = 5$ nm, the electric quadrupole transition is excited at a wavelength of $\lambda \approx 500$ nm and the electric dipole transition at $\lambda \approx 550$ nm. On the other hand, the quadrupole transition for a quantum dot of radius $a = 10$ nm occurs at $\lambda \approx 615$ nm and the electric dipole transition at $\lambda \approx 630$ nm.

For a quantum dot that is just beneath the exciting dipole ($\mathbf{r} = \mathbf{0}$), Fig. 91.48 shows the ratio of the quadrupole absorption rate and the dipole absorption rate ($\left\langle \alpha^Q \right\rangle / \left\langle \alpha^E \right\rangle$) as a function of the normalized separation z_0/λ. The vertical dashed line indicates the minimum physical distance between quantum dot and the dipole, i.e., the limit at which the tip and quantum dot would touch (we assume a tip radius of 5 nm).

For the quantum dot with radius $a = 5$ nm and an excitation wavelength of $\lambda = 550$ nm, the normalized minimum distance

is $z_0^{min}/\lambda \approx 0.018$. Similarly, for the quantum dot with radius $a = 10$ nm and a wavelength of $\lambda = 630$ nm, the minimum distance is 15 nm, which corresponds to a normalized distance of $z_0^{min}/\lambda \approx 0.024$. The important finding is that the ratio $(\langle\alpha^Q\rangle/\langle\alpha^E\rangle)$ can be as high as 0.3 for a 5-nm quantum dot [see Fig. 91.48(a)] and even 0.6 for a 10-nm quantum dot [see Fig. 91.48(b)]. These values are roughly three orders of magnitude larger than those obtained by using far-field excitation [for plane wave excitation the ratio is of the order of $(a/\lambda)^2$]. Thus, we find that in the extreme near field $(z_0 < \lambda/10)$, quadrupole transitions become important and the electric dipole approximation is not sufficiently accurate!

The plots in Figs. 91.49 and 91.50 are generated by scanning the quantum dot in the x-y plane while keeping the exciting dipole at the constant height z_0. Figure 91.49 shows the electric dipole absorption rate $\langle\alpha^E\rangle$, whereas Fig. 91.50 shows the electric quadrupole absorption rate $\langle\alpha^Q\rangle$. Both plots are symmetrical with respect to the z axis. In the case of $\langle\alpha^E\rangle$, this symmetry is generated by the dominant field component $\tilde{E}_z$, whereas in the case of $\langle\alpha^E\rangle$, the symmetry is due to the strong field gradient $\partial\tilde{E}_z/\partial z$. The electric dipole absorption rate is proportional to the square of the particle dipole moment p_0 and to the square of the lattice constant of the crystal d. On the other hand, the quadrupole absorption rate is also proportional to the square of (a/λ). This is evident in Fig. 91.50 where the ratio a/λ in Fig. 91.50(b) is twice the ratio a/λ in Fig. 91.50(a). A comparison between the widths of the curves in Figs. 91.49 and 91.50 shows that *no* improvement of spatial resolution can be achieved by selectively probing optical quadrupole transitions!

Conclusions

As was mentioned above, laser-irradiated metal tips are used in near-field optical microscopy as miniature light sources.[17] A strongly enhanced and localized optical field is created at the tip apex if proper polarization conditions are used. Using this technique, spectroscopic measurements with spatial resolutions of only 10 to 20 nm have been demonstrated.[17] To date, this is the highest spatial resolution of any optical spectroscopic measurement. This technique will be
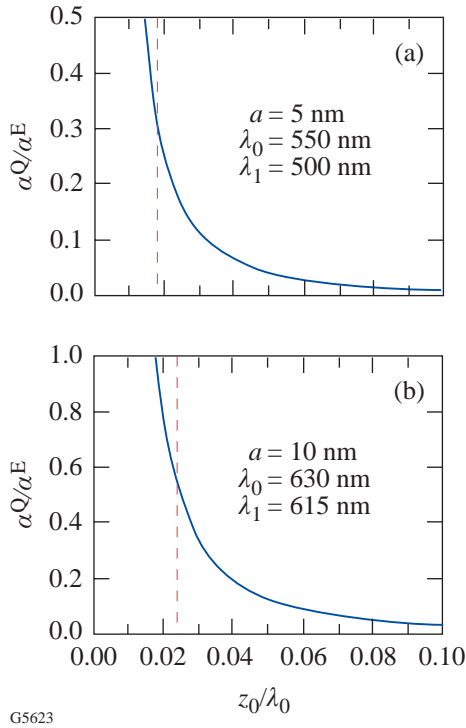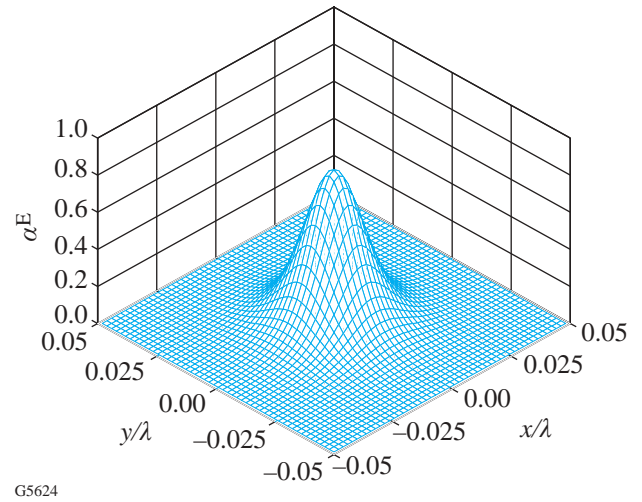

G5623

G5624

Figure 91.48
Ratio of the electric quadrupole absorption rate $\langle\alpha^Q\rangle$ and the electric dipole absorption rate $\langle\alpha^E\rangle$ as a function of the normalized distance (z_0/λ_0) between excitation dipole $(\mathbf{r}_0 = z_0\mathbf{n}_z)$ and quantum dot center $(\mathbf{r} = \mathbf{0})$. The quantum dot radius is $a = 5$ nm in (a) and $a = 10$ nm in (b). The vertical dashed line indicates the minimum physical separation between the center of the quantum dot and the exciting dipole. This separation corresponds to $a_t + a$, where $a_t = 5$ nm is the radius of curvature of the metal tip.

Figure 91.49
Electric dipole absorption rate $\langle\alpha^E\rangle$ as a function of the normalized lateral coordinates $(x/\lambda, y/\lambda)$. The height of the excitation dipole is $z_0 = 0.025\,\lambda$. The vertical axis has units of $(2\pi^2)(edp_0/\epsilon_0)^2[10^4/(\hbar\lambda^6)]\delta[\hbar\omega - (\epsilon_{10} + \epsilon_{10})]$. The symbols e, d, and p_0 denote the elementary charge, the lattice constant, and the dipole moment, respectively.

applied in our future investigations to experimentally verify the quadrupole transitions predicted in this work. Single CdSe quantum dots will be dispersed on a flat substrate, and the quantum dot luminescence will be recorded as a function of excitation wavelength and tip position.

In this work, higher-order multipole interactions between a semiconductor quantum dot and a strongly confined optical field have have analyzed. Expressions have been derived for the electric quadrupole interaction Hamiltonian, the associated absorption rate, and selection rules. It has been assumed that the quantum dot has a p-like valence band and an s-like conduction band. Also, the Bohr radii of electron and hole were assumed to be larger than the sphere radius (strong confinement limit), and no Coulomb interactions between hole and electron have been taken into account. Because of their different selection rules, electric dipole and electric quadrupole interband transitions can be separated and selectively excited. The electric quadrupole absorption strength depends on the bulk properties of the material (Bloch functions) as well as on the envelope functions (confinement functions). This differs from the electric dipole absorption strength, which depends only on the bulk properties of the semiconductor. When the quantum dot with radius a interacts with the confined optical field produced by a sharply pointed tip, the ratio between the electric quadrupole absorption rate and the electric dipole absorption rate can be as high as 0.3 for $a = 5$ nm and even 0.6 for $a = 10$ nm. Electric quadrupole transitions cannot be ignored in the extreme near field, i.e., for separations between tip and quantum dot smaller than $\lambda/10$. The inclusion of electric quadrupole transitions modifies the absorption spectra of quantum dots in the extreme near field. We have shown, however, that no improvement in the spatial resolution can be achieved by selective probing of electric quadrupole transitions. Future studies will be directed at electric quadrupole excitonic interactions.

REFERENCES

1. V. I. Klimov *et al.*, Science **290**, 314 (2000).

2. G. K. Brennen, I. H. Deutsch, and P. S. Jessen, Phys. Rev. A, At. Mol. Opt. Phys. **61**, 062309 (2000).

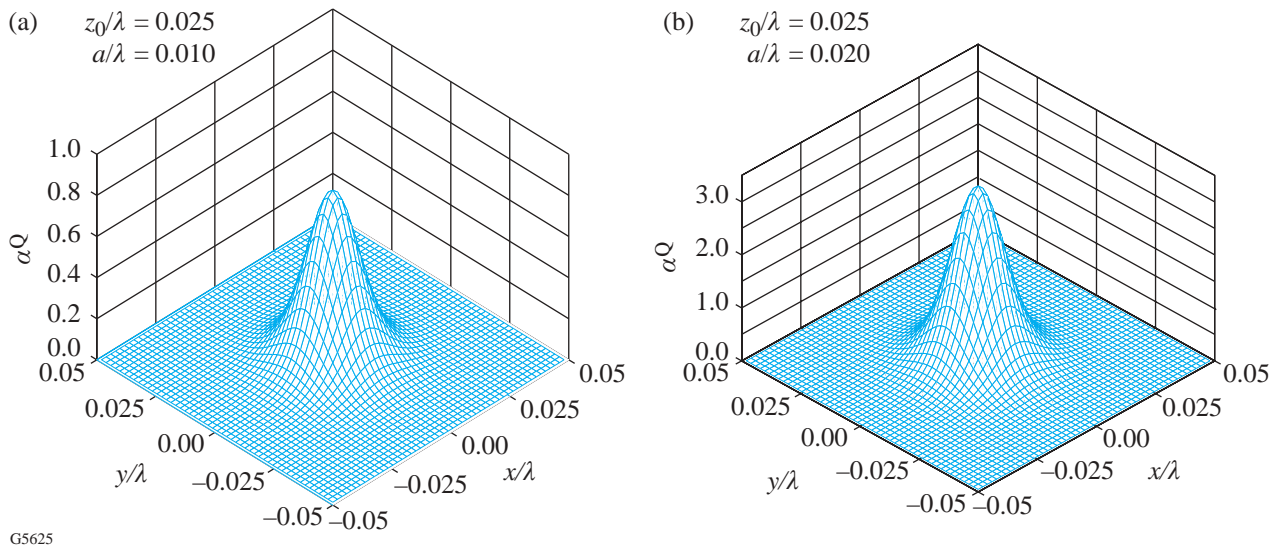3. P. Michler *et al.*, Science **290**, 2282 (2000).

G5625

Figure 91.50
Electric dipole absorption rate $\langle \alpha^Q \rangle$ as a function of the normalized lateral coordinates $(x/\lambda, y/\lambda)$. The height of the excitation dipole is $z_0 = 0.025\ \lambda$. The symbols e, d, and p_0 denote the elementary charge, the lattice constant, and the dipole moment, respectively. The quantum dot radius is $a = 0.01\ \lambda$ in (a) and $a = 0.02\ \lambda$ in (b). The width of the curve is roughly the same as in Fig. 91.49, which indicates that no improvement of resolution can be achieved by quadrupole transitions. The vertical axis has units of $\left(2\pi^5\right)\left(edp_0/\epsilon_0\right)^2\left[10^4/\left(\hbar\lambda^6\right)\right]\delta\left[\hbar\omega - \left(\varepsilon_{10} + \varepsilon_{11}\right)\right]$.

4. For a recent review, see R. C. Dunn, Chem. Rev. **99**, 2891 (1999).

5. N. Van Hulst, ed., J. Microsc. **202** (1, Pt. 1), 1 (2001).

6. R. D. Grober *et al.*, Appl. Phys. Lett. **64**, 1421 (1994).

7. J. Levy *et al.*, Phys. Rev. Lett. **76**, 1948 (1996).

8. A. Richter *et al.*, Ultramicroscopy **71**, 205 (1998).

9. A. von der Heydt *et al.*, J. Chem. Phys. **112**, 7831 (2000).

10. O. Mauritz *et al.*, Phys. Rev. Lett. **82**, 847 (1999).

11. A. Knorr, S. W. Koch, and W. W. Chow, Opt. Commun. **179**, 167 (2000).

12. B. Hanewinkel *et al.*, Phys. Rev. B, Condens. Matter **55**, 13,715 (1997).

13. G. W. Bryant, Appl. Phys. Lett. **72**, 768 (1998).

14. A. Chavez-Pirson and S. T. Chu, Appl. Phys. Lett. **74**, 1507 (1999).

15. H. F. Hamann *et al.*, J. Chem. Phys. **114**, 8596 (2001).

16. Y. C. Martin, H. F. Hamann, and H. K. Wickramasinghe, J. Appl. Phys. **89**, 5774 (2001).

17. E. J. Sanchez, L. Novotny, and X. S. Xie, Phys. Rev. Lett. **82**, 4014 (1999), and references therein.

18. L. Novotny, in *Near-Field Optics and Surface Plasmon Polaritons, Topics Appl. Phys.*, edited by S. Kawata (Springer-Verlag, Berlin, 2001), Vol. 81, pp. 123–141.

19. R. G. Woolley, J. Phys. B, At. Mol. Phys. **6**, L97 (1973).

20. L. D. Barron and C. G. Gray, J. Phys. A, Math. Gen. **6**, 59 (1973).

21. H. Haug and S. W. Koch, *Quantum Theory of the Optical and Electronic Properties of Semiconductors*, 2nd ed. (World Scientific, Singapore, 1993).

22. L. Banyai and S. W. Koch, *Semiconductor Quantum Dots*, World Scientific Series on Atomic, Molecular, and Optical Physics, Vol. 2 (World Scientific, Singapore, 1993).

23. C. Hafner, *The Generalized Multipole Technique for Computational Electromagnetics* (Artech House, Boston, 1990).

24. L. Novotny, R. X. Bian, and X. S. Xie, Phys. Rev. Lett. **79**, 645 (1997).

25. C. Tai, *Dyadic Green Functions in Electromagnetic Theory*, 2nd ed., IEEE Press Series on Electromagnetic Waves (IEEE Press, Piscataway, NJ, 1994).

26. P. Y. Yu and M. Cardona, *Fundamentals of Semiconductors: Physics and Materials Properties*, 1st ed., corr. print (Springer, Berlin, 1996).